CrossMark

REGULAR PAPER

**Nazri Md Daud · Yasuaki Kozato ·
Satoshi Kikuchi · Shigeki Imao**

Control of leading edge separation on airfoil using DBD plasma actuator with signal amplitude modulation

Abstract In this study, the separation control of an airfoil when a dielectric barrier discharge (DBD) plasma actuator is mounted on its leading edge was examined. Experiments were performed at a Reynolds number of approximately 67,000 with an external airflow of 10 m/s. The DBD plasma actuator was installed on an NACA 0015 airfoil with a 100 mm chord and 150 mm width at $x/c = 0.025$, where x was the vertical distance measured from the leading edge and c was the chord length. Lift force measurements, flow visualization and velocity measurements were conducted to investigate the performance of the DBD plasma actuator, which was driven by either pulse modulation with amplitude modulation (PM + AM) or pulse modulation only (PM). The PM + AM case was designed to consume the same amount of power as the PM case. The result showed that the PM + AM case improved the lift coefficient compared to the PM case for both St = 0.6 and St = 4.0. Under the stall control condition (angle of attack, $\alpha = 16°$) and high angle of attack condition ($\alpha = 18°$), the PM + AM case always demonstrated improved lift over the PM case; the improvement in lift was greater at $\alpha = 18°$ than at $\alpha = 16°$. Flow visualization confirmed larger and stronger vortex shedding for the PM + AM case over the PM case.

Keywords Plasma actuator · Airfoil · Separation control · Dielectric barrier discharge

List of symbols

A	Wing area
C_l	Lift coefficient $= L/(0.5\rho U_0^2 A)$
c	Chord length
Duty	Ratio of ON time to period of modulation actuation (duty ratio) $= T_{on}/T$
f_B	Base frequency
f_M	Modulation frequency $= 1/T$
L	Lift force
Re	Reynolds number $= U_0\,c/v$
St	Non-dimensional pulse modulation frequency $= f_M\,c/U_0$
T	Period of ON–OFF cycle

N. Md Daud (✉)
Graduate School of Engineering, Gifu University, 1-1, Yanagido, Gifu 501-1193, Japan
E-mail: r3812203@edu.gifu-u.ac.jp
Tel.: +81-58-293-2521

Y. Kozato
Department of Integrated Mechanical Engineering, Daido University, 10-3, Takiharu-cho, Minami-ku, Nagoya 457-8530, Japan

S. Kikuchi · S. Imao
Department of Mechanical Engineering, Gifu University, 1-1, Yanagido, Gifu 501-1193, Japan

T_{on}	Period that DBD plasma actuator is ON
U_0	Uniform flow velocity
u'	Root mean square value of fluctuating velocity
x, y	Horizontal and vertical distances measured from leading edge
α	Angle of attack
ρ	Air density
v	Kinematic viscosity of air

1 Introduction

Many researchers have studied using plasma actuators for the separation control of airfoils. Most of their studies were focused on using a dielectric barrier discharge (DBD) plasma actuator in various applications, such as separation control on an airfoil under laminar flow (Sosa and Artana 2006), actuator location optimization (Jolibois et al. 2008), airflow reattachment using a DBD actuator (Bernard et al. 2008), lift and drag improvement of airfoils (Bernard et al. 2009) and separation control using unsteady actuation (Amitay and Glezer 2002; Rethmel et al. 2011). Interest in DBD plasma actuator is growing because of their unique features such as no moving parts, quick response and extremely low mass. Other devices, e.g., mechanical slats and flaps, add more weight and produce noise on the aircraft.

A DBD plasma actuator consists of an exposed electrode and encapsulated electrode that are separated by a dielectric material. Plasma is created when sufficient voltage is applied between the exposed and encapsulated electrodes. The DBD plasma actuator is usually excited with an AC voltage to allow continuous plasma generation. Momentum is transferred from the plasma discharge to the ambient air through ion collision which creates an ionic wind or induced air flow. Forte et al. (2007) conducted Pitot tube measurements and obtained ionic wind velocities of up to 7 m/s at 0.5 mm from the wall for a single actuator and 8 m/s for multiple actuators. Meanwhile, Craig et al. (2010) developed a new configuration for plasma actuators. They claimed that the major problem with plasma actuators is the relatively low induced velocity of the jet. If the jet velocity can be increased, more momentum can be imparted to the flow. Therefore, increasing the jet velocity will make this device suitable for use over a wider range of Reynolds numbers. They studied the potential of multiple encapsulated electrodes (MEE) to increase the induced velocity. In their results, they were able to use MEE actuators to produce an induced velocity that was 36.5 % higher than the baseline case. However, a higher ionic velocity is not strictly related to improve flow control performance (Bernard et al. 2009). They found that unsteady actuation increases the aerodynamic performance of an airfoil compared to steady actuation. There is a strong suspicion that the vortex interaction has a larger influence on the improved results than the ionic velocity.

Balcon et al. (2009a) claimed that successful separation control at high angles of attack depends on vortex interaction due to the effects of an unsteady actuation or pulse modulation drive. This means that the DBD plasma actuator is triggered by on and off modes at a specific modulation frequency. For instance, a pulse modulation drive was successfully used to delay stall compared to the steady actuation case (Md Daud et al. 2014). This is because the pulse modulation drive may be able to cause a separated shear layer near the leading edge to roll up and develop. Asada et al. (2009) also reported that a smaller duty ratio provides stronger separation control capability despite a lower input energy. Jukes and Choi (2012) demonstrated that a DBD vortex generator develops streamwise vortices in their experiments. They successfully used their method to reduce the separation region. Therefore, the vortex interaction due to the actuation effect or actuator position is important for improving the flow control performance.

The electrical discharge of a DBD plasma actuator is powered by a sinusoidal waveform signal. However, Balcon et al. (2009b) modified the waveform signal. They studied the effect of positive and negative sawtooth signals on electric wind. Bernard and Moreau (2010) demonstrated the capabilities of plasma actuators by adjusting the voltage waveform into burst, superposition and ring modulation signals. In the present study, we applied a signal comprising pulse modulation and amplitude modulation (PM + AM) to a DBD plasma actuator. In this case, the DBD plasma actuator was placed near the leading edge of the NACA 0015 airfoil model. The objective of this study was to improve the lift coefficient compared to the result of a previous experiment (Md Daud et al. 2014). In this previous experiment, a pulse modulation drive with a constant voltage amplitude signal was applied under a high angle of attack condition. We compared the results to examine the flow pattern when both the pulse and amplitude are modulated.

2 Experimental setup

The experimental apparatus used in this study was the same as that used in our previous study (Md Daud et al. 2014). Figure 1 shows an overview of the experimental setup. The experiment was conducted in a low-speed, semi-closed wind tunnel with a square cross-section having dimension of 500 mm × 500 mm. An NACA 0015 airfoil with a chord length of 100 mm and span of 150 mm was tested at $Re \approx 67,000$ in an airflow of 10 m/s. The DBD plasma actuator was installed at $x/c = 0.025$ of the chord length.

The DBD plasma actuator consisted of two copper-tape electrodes; each electrode was 50 µm thick and 5 mm wide. The two electrodes (exposed and encapsulated) were arranged in parallel with a 1 mm overlap. These electrodes were separated by a 100 µm thick Kapton film that acted as a dielectric.

The lift force was measured directly with a load cell (LMC-3501-50N, Nissho Electric Works, Japan) having a rated load of 50 N and accuracy of ±0.2 %. The sampling frequency was set to 1 kHz with a low-pass filter of 10 Hz over approximately 4 s. The velocity was measured at the mid-span of the airfoil with an I-type hot-wire probe and constant temperature anemometer. The sampling frequency was 50 kHz, the measurement time was approximately 4 s and electromagnetic noise was removed with a 2 kHz low-pass filter. The thermal effect caused by the plasma generation seemed to be small, because the measurements were conducted at a distance from the plasma actuator. Therefore, the values measured by the hot-wire probe were obtained without any compensation. The output signal from the anemometer was converted with an A-D converter (WE7000, Yokogawa, Japan), after which a customized LabVIEW program processed the data.

The flow was visualized with a high-speed camera (GX 8, nac Image Technology, Japan) and continuous laser sheet (SVL-532-1000-45L, Sanctity Laser, China). The laser sheet intersected the airfoil at its mid-span, and the axis of the high-speed camera was oriented perpendicular to that of the laser sheet. The camera frame rate was 2000 fps, and its resolution was 1024 × 768 pixels. In the experiment, smoke was produced by the smoke wire method, and the airflow speed was set to 5 m/s. The quantity of nickel powder used as seeding particles was so small that its effect on the flow was not detected even near electrodes. In the results, the Reynolds number for the flow visualization was half that used in our other experiments. However, the trend of the aerodynamic performance did not vary significantly, especially for St = 0.6 and St = 4.0.

2.1 Pulse modulation

In our previous experiment (Md Daud et al. 2014), a high-voltage AC current was supplied to the exposed electrode while the encapsulated electrode was grounded. The base waveform was an 8 kHz sinusoidal wave, generated by a digital function generator (DF1906, NF Corporation, Japan). The signal was amplified by a high-voltage amplifier (HEOPT-10B10-LI, Matsusada Precision Inc., Japan) to provide a peak-to-peak voltage of 6 kV. Unsteady actuation was performed through the application of a low modulation frequency to the base wave. Figure 2 shows the ON–OFF controlled waveforms for the PM case at St = 0.6 and St = 4.0.
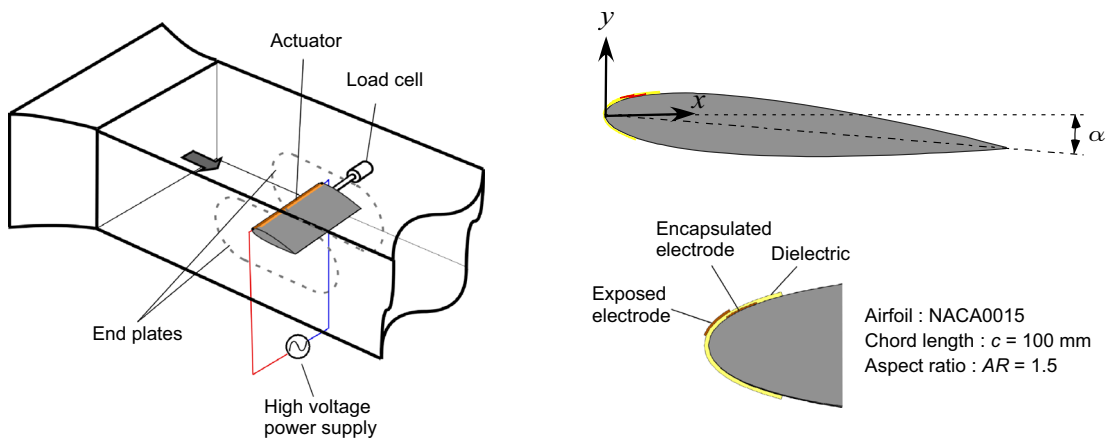
Fig. 1 Experimental setup using airfoil model NACA 0015 in a low-speed, semi-closed wind tunnel with $Re \approx 67,000$ and an airflow velocity of 10 m/s
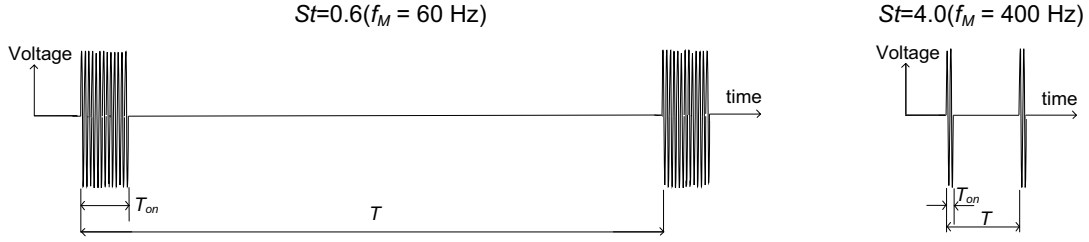
Fig. 2 Waveforms for the PM case (f_B = 8 kHz, Duty 10 %)

2.2 Amplitude modulation

In this experiment, the PM + AM case was designed to have the same power consumption as the PM case. The power consumption was measured with the electric current method proposed by Ashpis et al. (2012). The time series of the voltage and current signals was recorded with a GW Instek GDS-2062 oscilloscope (8 bits, 60 MHz bandwidth, 1 GS/s/channel @ 2 active channels). 12,500 samples of data were recorded at 0.25 MHz sampling frequency for St = 0.6 and 1.25 MHz sampling frequency for St = 4.0. These were the suitable sampling frequency to obtain low amplitude current spikes. A resistor with a known resistance, $R = 100\ \Omega$, was placed in series between the exposed electrode and ground to calculate the current. The applied voltage was calculated from the monitored output of high-speed and high-voltage amplifier. The PM + AM case was designed using DF0106 software (NF Corporation, Japan). The waveform of the PM + AM case was set with the same modulation frequency f_M and same base frequency f_B as that of the PM case. In the results, the T_{on} and T periods were the same for the PM + AM and PM cases. Thus, the power consumptions for the PM and PM + AM cases were about 0.46 W when St = 4.0 and 0.36 W when St = 0.6. From our result, we concluded that the power consumption is only proportional to V_{p-p} if St is less than 2.0.

When St = 0.6, there were 13 cycles of the base wave within one ON time period, while only two cycles of base waves existed when St = 4.0; this is shown in Fig. 2. We set a maximum voltage of 7 kV and minimum voltage of 5 kV for the St = 0.6 case, while a maximum voltage of 7 kV and minimum voltage of 2 kV were used for the St = 4.0 case. This is a suitable maximum voltage because a maximum voltage of greater than 7 kV will cause the Kapton film to become damaged more easily. In addition, obtaining the same power consumption as in the PM case is difficult, if the maximum voltage is lower than 7 kV. Figure 3 shows waveforms for the PM + AM case with decreasing and increasing patterns. The results obtained for each pattern were compared (not shown), and the lift coefficient C_l of the decreasing pattern was found to be slightly better than that of the increasing pattern, although the difference was very small. Therefore, we adopted a decreasing amplitude modulation in this study. It is also important to highlight that in the case of St = 4.0 which has two cycles, it is not proper to express it as amplitude modulation. This is an extreme and rare case in the case of amplitude modulation.

3 Results and discussion

3.1 Effect of PM and PM + AM on lift coefficient

Figure 4 shows the lift coefficient C_l plotted against the angle of attack α. In the PM case, C_l increased compared with the Duty 100 % case in the previous study (Md Daud et al. 2014). However, the PM + AM case showed larger values of C_l compared to the PM case for both St = 0.6 and St = 4.0. Here, St is the non-dimensional pulse modulation frequency. For Duty 100 %, the airfoil stalled at $\alpha = 15°$, while C_l continued to increase to a high attack angle when PM or PM + AM was applied. In this experiment, the duty ratio was set to 10 % based on the results obtained by Asada et al. (2009). They found that the most effective duty ratio setting for the pulse modulation drive is 10 %.

The PM and PM + AM cases produced similar trends for C_l when St was the same. When St = 4.0, C_l decreased sharply after the maximum point, while C_l decreased gradually when St = 0.6. In the previous study, we examined the St = 0.6 and 4.0 cases under the stall control condition ($\alpha = 16°$) and at a high angle of attack ($\alpha = 18°$). Therefore, we applied the same condition to the PM + AM case. In this paper,
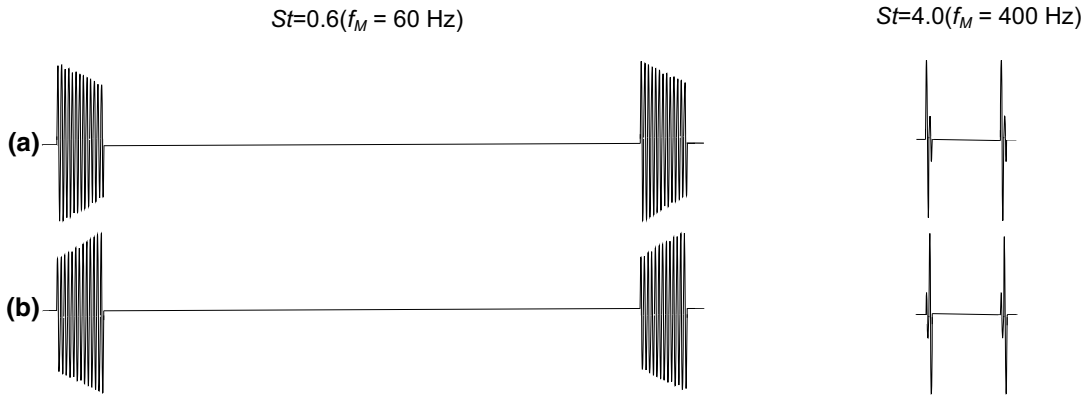
Fig. 3 Waveforms for the PM + AM case ($f_B = 8$ kHz, Duty 10 %) *a* decreasing pattern *b* increasing pattern
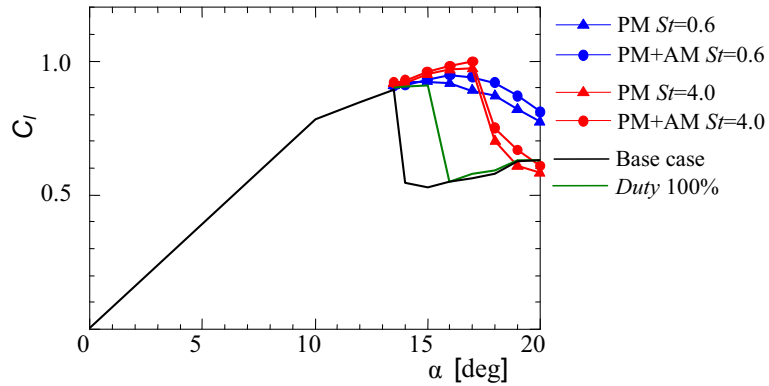

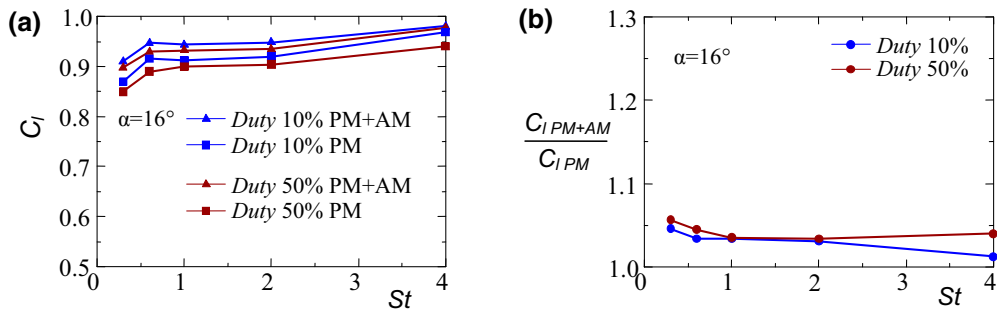**Fig. 4** The effect of PM and PM + AM cases on lift coefficient C_l for Duty 10 %

Fig. 5 Effect of modulation frequency on C_l at $\alpha = 16°$ (stall control condition)
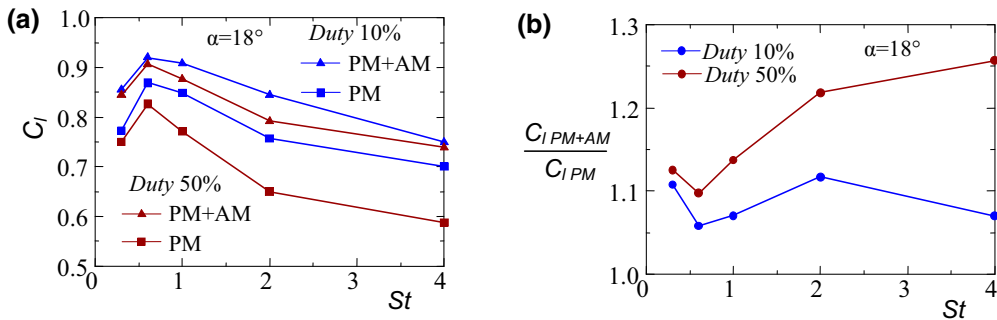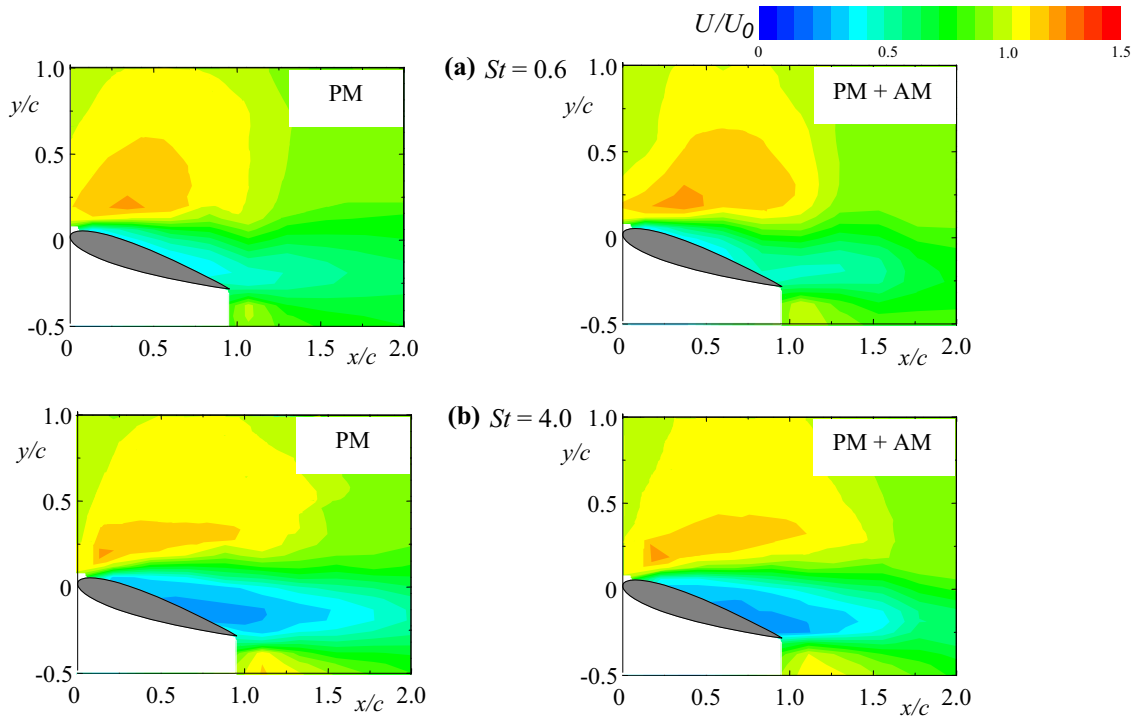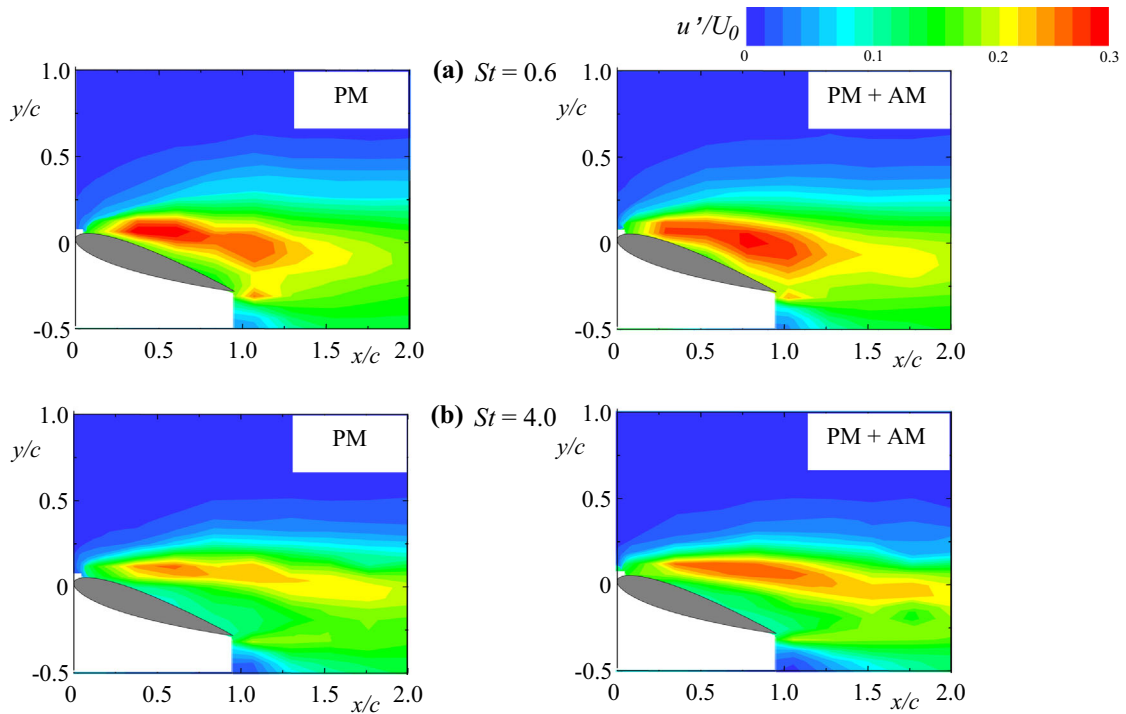

**Fig. 6** Effect of modulation frequency on C_l at $\alpha = 18°$ (high angle of attack condition)

Fig. 7 Time–mean velocity contour map at $\alpha = 18°$ for Duty 10 %

Fig. 8 Turbulence intensity contour map at $\alpha = 18°$ for Duty 10 %

the stall control condition is defined as the parameter set for which no stall occurs and C_l increases beyond the stalled point of the base case, ($\alpha = 16°$).

Figure 5a shows the lift coefficient C_l plotted against St at $\alpha = 16°$. Figure 5b shows the ratio of C_l for PM + AM to that for PM as a function of St. At the stall control condition ($\alpha = 16°$), C_l gradually increased
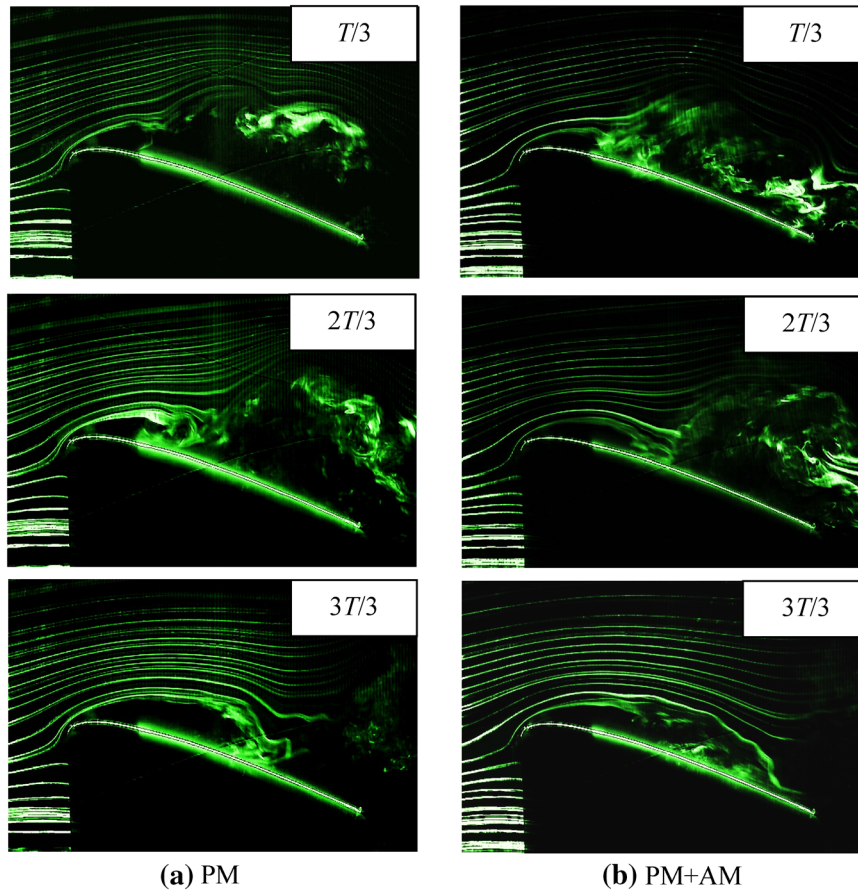
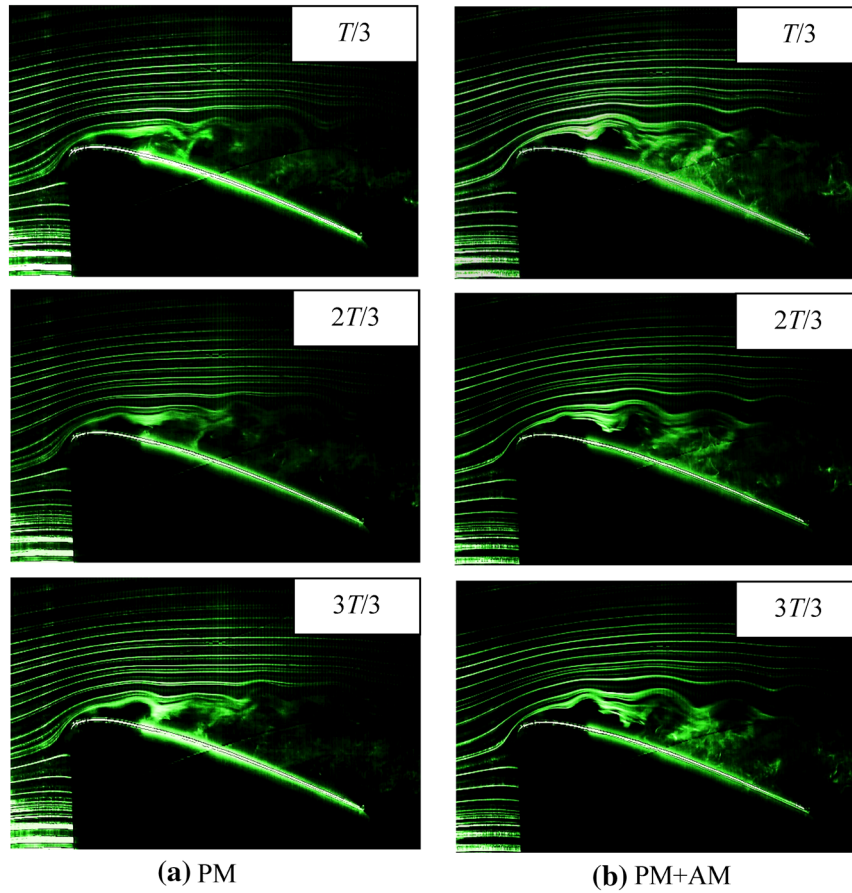**Fig. 9** Captured images of airflow over an airfoil at $\alpha = 18°$ when St = 0.6 (Duty 10 %)

with an increase in St and the PM + AM case showed little improvement in C_l compared to the PM case for each duty ratio. C_l was a few percentage points greater for the PM + AM case than for the PM case for all St. On the other hand, at a high angle of attack ($\alpha = 18°$) as shown in Fig. 6, C_l reached a local maximum and then rapidly decreases as St increased.

At $\alpha = 18°$, C_l was again greater for the PM + AM case than for the PM case for all St, but the rate of increase was greater than that at $\alpha = 16°$. The rate of increase in C_l was less than 5 % at $\alpha = 16°$, while it was greater than 5 % at $\alpha = 18°$. It reached 25 % when Duty 50 % and St = 4.0. PM + AM was clearly more effective than PM at improving the lift coefficient at high angles of attack.

3.2 Flow around airfoil

We examined the flow around the airfoil by focusing on the effect of PM + AM on C_l at a high angle of attack ($\alpha = 18°$). Figure 7 shows the mean velocity contour map when St = 0.6 and St = 4.0 for both of the PM and PM + AM cases. The mean velocities near the airfoil surface for the PM and PM + AM cases were almost the same when St = 0.6. However, the low velocity region at the suction side was slightly narrower for the PM + AM case. This situation occurred in the same manner when St = 4.0, where the low velocity region for the PM case was slightly wider compared to the PM + AM case. This indicates that the flow can be expected to attach slightly closer to the airfoil surface in the PM + AM case compared to the PM case when St = 0.6 and St = 4.0. The flow around the airfoil was also analyzed based on the results of the captured images for the velocity fluctuation and flow.

Figure 8 shows the turbulence intensity contour map for the PM and PM + AM cases when St = 0.6 and St = 4.0. When St = 0.6, a high level of turbulence intensity for the PM case was only detected near the leading edge and mid-point area of the airfoil surface. However, for the PM + AM case, a high level of turbulence was detected across the entire airfoil surface from the leading edge to the trailing edge. This was
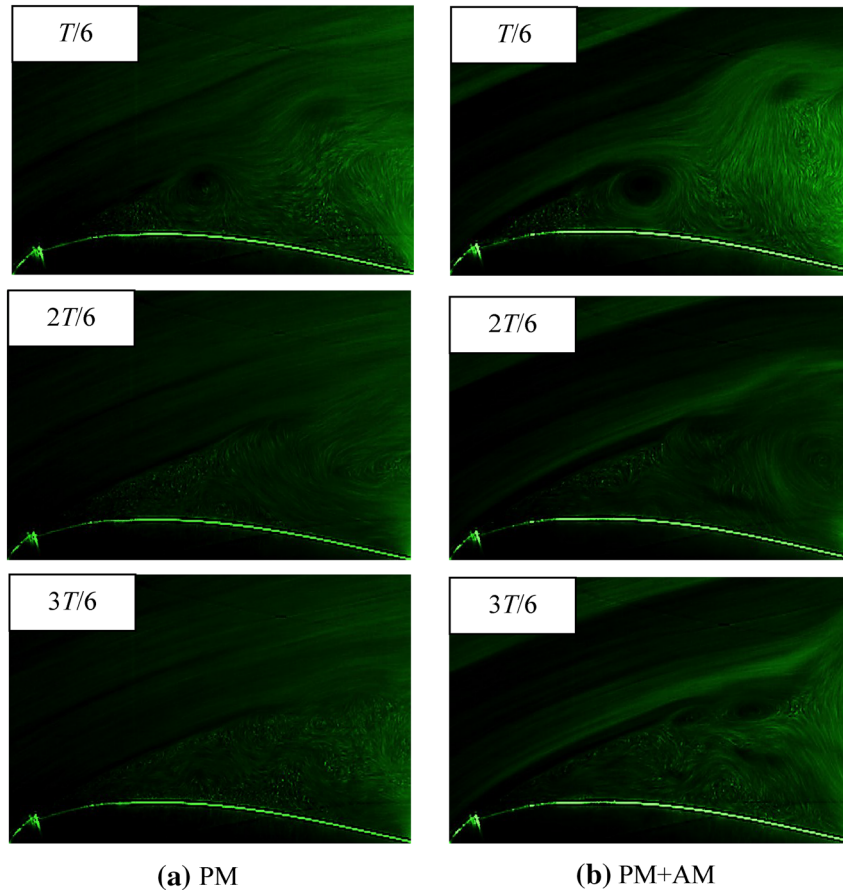
Fig. 10 Captured images of airflow over an airfoil at $\alpha = 18°$ when St = 4.0 (Duty 10 %)

due to the strong vortex shedding near the leading edge, which grew to a large vortex and flowed downstream along the airfoil surface. In other words, when St = 0.6, the PM + AM case is predicted to produce larger and stronger vortices near the leading edge and entire airfoil surface compared to the PM case. This larger vortex may be caused by the amplitude modulated actuation of the actuator. For St = 4.0, however, the region with a high level of fluctuating velocities was limited to near the leading edge. The turbulence intensity near the leading edge was slightly lower for the PM case than for the PM + AM case. The vortex produced from the leading edge should be much stronger for the PM + AM case than for the PM case.

Figures 9 and 10 use smoke wire to visualize St = 0.6 and St = 4.0, respectively, at a high angle of attack. Here, T is the period of one ON–OFF cycle. Flow separation occurred for all cases under these conditions. For St = 0.6, the separated shear layer rolled up and developed into a small-scale vortex at the leading edge during the $T/3$ period. The vortex scale became larger during the $2T/3$ and $3T/3$ periods in the middle area of the airfoil surface for the PM case (Fig. 9a). For the PM + AM case (Fig. 9b), the separated shear layer rolled up more definitely and developed into a vortex near the leading edge, which caused the vortex structure to become larger during the $T/3$ period. The growing vortex rolled downstream over the entire airfoil surface during the $2T/3$ and $3T/3$ periods. As a result, the lift coefficient was higher for the PM + AM case than for the PM case because of the growing vortex, which forced the flow closer to the wing surface.

For St = 4.0, the separation area appeared to be broader for both the PM and PM + AM cases. For the PM case, a small vortex structure was detected near the leading edge during the $T/3$ and $2T/3$ periods. Then, the vortex dispersed downstream during the $3T/3$ period. On the other hand, for the PM + AM case, the separated shear layer near the leading edge rolled up and grew to a slightly larger-scale vortex than that in the PM case during the $T/3$ period. The large vortex rolled near the wing surface over the mid-area of airfoil during the $3T/3$ period.

(a) PM   **(b)** PM+AM

Fig. 11 Captured images of airflow over the leading edge of an airfoil at $\alpha = 18°$ when St = 0.6 (Duty 10 %)

To distinguish the results of the PM and PM + AM cases shown in Figs. 9 and 10 (especially for St = 4.0), the flow on the leading edge of the airfoil was visualized. Figures 11, 12 and 13 show images of the leading edge of the airfoil visualized with the smoke method. As shown in Fig. 11, when St = 0.6, the vortex shedding at the leading edge increased in size and flowed downstream (PM and PM + AM). After 3T/6, the vortex was no longer seen in these images. However, during the T/6 periods, the starting vortex was slightly larger for the PM + AM case than for the PM case (Fig. 11). This was due to the unsteady amplitude modulated from the PM + AM signal, which created a massive change in the separated shear layer near the leading edge. This stimulated the vortex strength which forced the flow closer to the wing surface. This agreed with the results presented in Fig. 8 (PM + AM) when St = 0.6. In addition, the movement of the vortex was much faster when the PM + AM case was applied to the actuator. This result is consistent with that shown in Fig. 9 during the 3T/3 period. The vortex covered up to 90 % of the wing surface for the PM + AM case, but only 70 % for the PM case during this period.

When St = 4.0 with a shorter period than in the St = 0.6 case, almost all vortex structures were captured in these images (Figs. 12, 13). The vortex size in both cases (PM and PM + AM) was the same during the T/6 and 2T/6 periods. However, for the PM + AM case, the unsteady amplitude modulated signal caused a rapid change in the separated shear layer. As a result, the vortex size became slightly larger as the starting vortex combined with the secondary vortex during the 3T/6 period (Fig. 13). Therefore, the combined vortices flowed slightly closer to the wing surface compared to the PM case. This result supports the findings shown in Fig. 8b, where the vortex near the leading edge was stronger rather than in the PM case. Therefore, the lift coefficient was higher for the PM + AM case than for the PM case. Overall, the lift variation is seemed to be influenced mainly by the amplitude modulation when St is low and it is influenced not only by the amplitude modulation but also by power consumption when St becomes high.
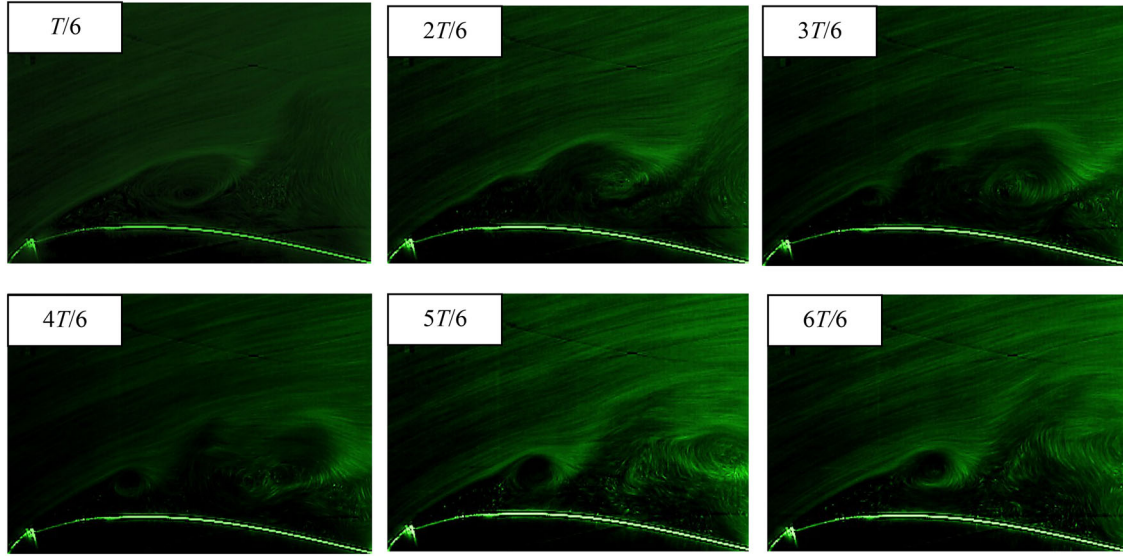
Fig. 12 Captured images of airflow over the leading edge of an airfoil for the PM case when St = 4.0 (α = 18°, Duty 10 %)
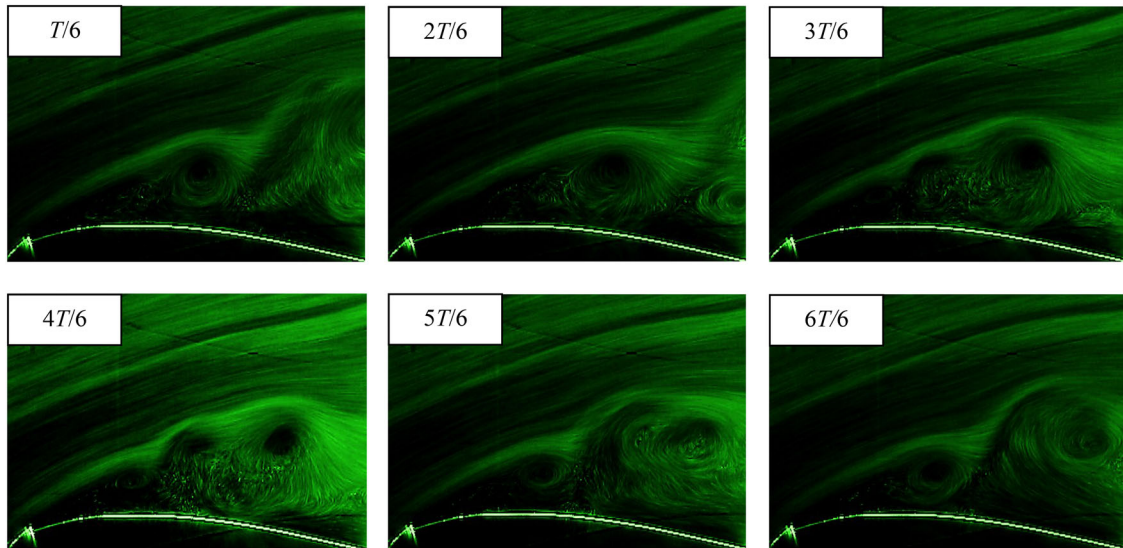
Fig. 13 Captured images of airflow over the leading edge of an airfoil for the PM + AM case when St = 4.0 (α = 18°, Duty 10 %)

4 Conclusion

An experimental study was performed to investigate the impact on the lift coefficient C_l of an amplitude modulated signal, applied to a DBD plasma actuator mounted on the leading edge of an NACA 0015 airfoil. The results are summarized as follows:

1. The lift coefficient C_l showed similar trends for both the PM and PM + AM cases at the same St values. When St = 4.0, C_l decreased rapidly after reaching a maximum. However, when St = 0.6, C_l decreased gradually.
2. The PM + AM case improves the lift coefficient more effectively than the PM case at a high angle of attack (α = 18°), with minimal improvement under the stall control condition (α = 16°).
3. An unsteady amplitude modulated signal stimulates vortex growth more for the PM + AM case than for the PM case; the former forces the flow closer to the wing which improves the lift coefficient.

References

Amitay M, Glezer A (2002) Role of actuation frequency in controlled flow reattachment over a stalled airfoil. AIAA J 40(2):209–216

Asada K, Ninomiya Y, Oyama A, Fujii K (2009) Airfoil flow experiment on the duty cycle of DBD plasma actuator, AIAA paper 2009-531, 47th AIAA aerospace sciences meeting

Ashpis DE, Laun MC, Griebeler EL (2012) Progress towards accurate measurements of power consumptions of DBD plasma actuators, AIAA paper 2012-0823, 50th AIAA aerospace science meeting

Balcon N, Benard N, Moreau E (2009a) Formation process of the electric wind produced by a plasma actuator. IEEE Trans Dielectr Electr Insul 16(2):463–469

Balcon N, Bernard N, Lagmich Y, Boeuf JP, Touchard G, Moreau E (2009b) Positive and negative sawtooth signals applied to a DBD plasma actuator—influence on the electric wind. J Electrostat 67:140–145

Bernard N, Moreau E (2010) Capabilities of dielectric barrier discharge plasma actuator for multi-frequency excitations. J Phys D Appl Phys 43:145201

Bernard N, Moreau E (2011) On the vortex dynamic of airflow reattachment forced by a single non-thermal plasma discharge actuator. Flow Turbul Combust 87:1–31

Bernard N, Braud P, Jolibois J, Moreau E (2008) Airflow reattachment along a NACA 0015 airfoil by surfaces dielectric barrier discharge actuator—time resolved particle image velocimetry investigation, AIAA paper 2008-4202, 4th flow control conference

Bernard N, Jolibois J, Moreau E (2009) Lift and drag performances of an axisymmetric airfoil controlled by plasma actuator. J Electrostat 67:133–139

Craig H, Rasool E, Konstantinos K (2010) Plasma actuators with multiple encapsulated electrodes to influence the induced velocity, AIAA paper 2010-1223, 43th AIAA aerospace sciences meeting

Forte M, Jolibois J, Pons J, Moreau E, Touchard G, Cazalens M (2007) Optimization of a dielectric barrier discharge actuator by stationary and non-stationary measurements of the induced flow velocity: application to airflow control. Exp Fluids 43:917–928

Jolibois J, Forte M, Moreau E (2008) Application of an AC barrier discharge actuator to control airflow separation above a NACA 0015 airfoil: optimization of the actuation location along the chord. J Electrostat 66:496–503

Jukes TN, Choi KS (2012) Dielectric barrier discharge vortex generators: characterization and optimization for flow separation control. Exp Fluids 52:329–345

Md Daud N, Kozato Y, Kikuchi S, Imao S (2014) Control of leading edge separation on airfoil using DBD plasma actuator. J Fluid Sci Technol 9(3)

Post ML, Corke T (2004) Separation control on high angle of attack airfoil using plasma actuators. AIAA J 42(11):2177–2178

Rethmel C, Little J, Takashima K, Sinha A, Adamovich I, Samimy M (2011) Flow separation control over an airfoil with nanosecond pulse driven DBD plasma actuators, 49th AIAA aerospace sciences meeting

Sosa R, Artana G (2006) Steady control of laminar separation over airfoils with plasma sheet actuators. J Electrostat 64:604–610